Tuning the structure, stability and responsivity of polymeric arsenical nanoparticles using polythiol cross-linkers

Joji Tanaka,[†] Guillaume Moriceau,[†] Alexander Cook,[†] Andrew Kerr,[†] Junliang Zhang,[†] Raoul Peltier,[†] Sebastien Perrier,[†] Thomas P. Davis,[§] Paul Wilson[†§]*

[†]Department of Chemistry, University of Warwick, Library Road, CV4 7AL Coventry, United Kingdom

[§]ARC Centre of Excellence in Convergent Bio-Nano Science and Technology, Monash Institute of Pharmaceutical Sciences, Monash University (Parkville Campus), 399 Royal Parade, Parkville, Victoria 3152, Australia

TABLE OF CONTENTS GRAPHIC ONLY

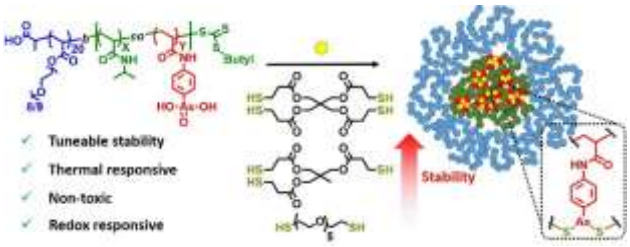

ABSTRACT

The use of organic arsenicals in polymer chemistry and biomaterials science is limited despite the distinctive and versatile chemistry of arsenic. The interchangeable oxidation states of arsenic and the subsequent changes in chemical properties makes it a promising candidate for redox responsive materials. Thus, reversible addition fragmentation chain transfer (RAFT) polymerization has been employed for the first time to synthesize thermoresponsive organic arsenical containing block copolymers. The polymers undergo simultaneous self-assembly and cross-linking, via the organic arsenical pendant groups, under reductive conditions (to reduce As(V) to As(III)) in the presence of polythiol reagents as cross-linkers. The formation of As-S bonds stabilises the nanoparticles formed (D_h = 19 - 29 nm) and enables the stability and responsivity to oxidative stress of the particles, in aqueous and model biological solutions, to be tuned as a function of the number of thiols in the cross-linker or the [SH]/[As] stoichiometric ratio. The parent block copolymers and nanoparticles are non-toxic *in vitro* and the tuneable responsivity of these nanoparticles and the (bio)chemical activity of organic arsenical reagents could be advantageous for targeted drug delivery and the other bio(nano)medical applications. To the best our knowledge, this is the first time that arsenic-thiolate (As-S) bonding has been employed for stimuli responsive cross-linking of polymeric nanoparticles.

INTRODUCTION

Self-assembly of block copolymers is an established method for the fabrication of polymeric nanomaterials.[1] Fundamental research into the relationship between block copolymer composition and self-assembled morphology,[2] in both bulk and solution, has facilitated the development of a new field of applied science with applications in fields including bio(nano)medicine,[3] biomaterials,[4] nanotechnology[5] and catalysis,[6] amongst others. Progress in both fundamental and

applied research has been driven by advances in synthetic methods that enable the synthesis of block copolymers with exquisite control over the molecular weight and molecular weight distribution of each block. Living anionic polymerization[7] provides optimal control over polymerization leading to discrete domains which can efficiently phase separate depending on the monomers employed. However, the sensitive nature of anionic polymerization limits the functional scope of the monomers that can be employed. The discovery and development of reversible deactivation radical polymerization (RDRP) techniques such as; reversible addition fragmentation chain transfer polymerization (RAFT),[8] nitroxide mediated polymerization (NMP)[9] and transition metal mediated methods *e.g.* atom transfer radical polymerization (ATRP)[10] and single electron transfer living radical polymerization (SET-LRP),[11] has addressed this limitation and greatly expanded the functional group tolerance. Furthermore, the most recent developments of these protocols allows the synthesis of (multi) block copolymers with excellent control over block copolymer composition in a variety of architectures including linear,[12] telechelic,[13] star[14] and cyclic/tadpole-shaped[15] polymers.

The behaviour of amphiphiles in aqueous solution can be rationalized from a thermodynamic perspective whereby interfacial interactions of the insoluble components are minimized, resulting in lower interfacial free energy. Under thermodynamic control, the position of equilibrium and therefore the stability or morphology of self-assembled block polymers can be manipulated by changes in concentration and temperature.[16] In the context of bio(nano)medicine applications, a key property of self-assembled block copolymers is the stability of the resulting nanoparticles under the high dilution conditions imposed *in vivo*.[17] The relative stability of self-assembled amphiphiles can be inferred from the critical aggregation concentration (CAC),[18] which is typically much lower for polymeric nanoparticles than those formulated using small molecule

amphiphiles (*e.g.* phospholipids). The stability can be further tuned according to the properties imposed by the monomers constituting the core and corona-forming blocks. For example, decreasing chain mobility (*i.e.* increasing T_g) within the core forming block can lead to kinetic trapping during self-assembly, which is the basis for crystallization-driven self-assembly.[19] Furthermore, non-covalent interactions such as hydrophobic,[20] π-π[21] or electrostatic interactions,[22] as well as hydrogen bonding[23] and transition metal complexation[24] can provide additional stabilization within core-forming blocks.

Alternatively, cross-linking through the formation of covalent bonds within the core[25] and/or the corona,[26] can result in enhanced stability. Covalent cross-linking results in the formation of either static (irreversibly) or dynamic bonds. The latter confers the potential for reversibility and responsivity, which can be engineered into polymers using functional vinyl-monomers compatible with RDRP protocols. For example, aldehydes/ketones for formation of imines,[27] oximes[28] and hydazones,[29] as well as disulfides[30] and boronic acid/boronate esters[31] are functional monomers that can respond to biological stimuli such as pH, redox and/or other specific biomarkers/biomolecules such as reactive oxygen species (ROS),[32] sugars[33] and enzymes.[34] The ability to control stability in biological media and responsivity to biological stimuli is an important property to consider for drug delivery and other bio(nano)medical applications.[35] Through this it is possible to manipulate release profiles, pharmacokinetics/dynamics of active pharmaceutical ingredients and also prevent synthetic materials from accumulating in the body which often correlates to lower toxicity.[36]

Organic arsenicals are interesting candidates for dynamic cross-linking owing to the distinct reactivity arising from their interchangeable oxidation states (As(V) - As(III) – As(I)). The first example of this traces back to the first organic arsenical chemotherapeutic, arsphenamine

(Salvarsen), which is synthesized by reductive coupling of a monomeric organic arsenic acid (As(V)) reagent, and exists as homocyclic oligomers ($As(I)_n$) comprised of multiple As-As bonds.[37] The As-As bonds are prone to hydrolysis and oxidation and the first investigation into stabilizing nanoparticles derived from diblock copolymeric arsenicals explored the stability and responsivity of such particles in aqueous and model biological media (5 mM glutathione, GSH/H_2O_2).[38] It was shown that the aqueous stability increased and that the responsivity to GSH could be tuned as a function of the arsenic mole fraction within the polymer composition. Conversely, under simulated oxidative stress in the presence of H_2O_2, all the particles disassembled rapidly (< 1 hour) highlighting the lability of these formulations to hydrolysis and oxidation.

In the case of arsphenamine, it is proposed that hydrolysis and oxidation of the As-As bonds is the mechanism for release of the active chemotherapeutic, which is thought to be a monomeric organic arsenous acid (As(III)) derivative. This hypothesis arises from the high affinity of As(III) for thiols, particularly proximal dithiols present in intracellular redox active proteins,[39] whereupon binding to As(III) can disrupt redox homeostasis,[40] induce mitochondrial dysfunction[41] that ultimately leads to cell death.[42] This has been exploited to develop organic arsenical based chemotherapeutics.[43] The thermodynamics[44] and nucleophilic exchangeability of arsenic-thiolate (As-S) bonding is well known, and is the basis for pro-fluorescent *bis*-arsenicals that bind to tetracysteine motifs through thiol exchange with ethane dithiol adducts.[45] From a biomaterials perspective this has been exploited to develop functional polymer scaffolds for post-polymerization modification,[46] highly specific, efficient and reversible approach to protein/peptide conjugation,[47] and nanoparticles presenting organic arsenical drugs as ligands for mitochondrial targeting.[48] However, the affinity, efficiency and nucleophilic exchangeability of the arsenic-thiolate interaction is yet to be investigated as a strategy for cross-linking to formulate,

stabilize and tune the responsivity of polymeric nanoparticles. Herein, polythiol reagents are investigated as cross-linkers for simultaneous self-assembly and cross-linking of thermoresponsive block copolymeric arsenicals. The structure, stability and responsivity to thiol exchange and simulated oxidative stress is investigated relative to the labile As-As cross-linked system with a view to employing such particles for stimuli responsive drug delivery and other bio(nano)medical applications in the future.

MATERIALS AND METHODS

General procedure for RAFT polymerisation (for P1p)

A typical synthesis of the first block is the following: CTA PABTC (24.8 mg, 0.1 mmol), $PEGA_{480}$ (1000 mg, 2.1 mmol), V601 (0.5 mg, 2.2 μmol) and trifluoroethanol (1.5 mL, 1 M monomer concentration) was charged into a vial equipped with a magnetic stirrer, the vial was then sealed with rubber septum and deoxygenated by a stream of bubbling nitrogen for 15 minutes with stirring. The vial was suspended in a preheated oil bath at 65 °C for 24 hrs. Reaction progress was monitored by ^{1}H NMR and SEC. No purification was required before chain extension.

A typical chain extension (for P1p)

The vial with reaction mixture containing the first block (macroCTA) was cooled before opening to air. NIPAm (1136 mg, 10 mmol), AsAm(pin_2) (644 mg, 1.4 mmol), V601 (1.26 mg, 5.5 2.2 μmol) and trifluoroethanol (3.8 mL, 3 M monomer concentration) were added and the mixture was well stirred. The vial was then re-sealed with a rubber septum and deoxygenated by a stream of bubbling nitrogen for 15 minutes with stirring. The vial was suspended in a preheated oil bath at 65 °C for 24 hrs. Reaction progress was monitored by ^{1}H NMR and SEC. No purification was required before deprotection.

Deprotection AsAm(pin)$_2$ units / removal of pinacol groups (P1 and P2)

The polymerisation reaction mixture (**P1p** / **P2p**) was dialysed in 0.1 M HCl solution overnight before changing to deionised water and further dialysed for 24 hours in deionised water, changing the water up to 3 times. The dialysed polymer solution was lyophilised to yielded **P1** as white powder (2.4 g, 85 % yield). Similarly, **P2** was obtained as white powder (2.0 g, 94 % yield).

General Procedure for Arsenic-thiolate cross-linked nanoparticle synthesis

AsAm functional polymer (**P1**/**P2,** 100 mg) was dissolved in deoxygenated aqueous solution (10 mL) of hypophosphorous acid (H_3PO_2, 10 wt%, 10 mg/mL polymer) and deoxygenated KI (1 vol% from a 3 wt % aq solution) was added. The solution was heated at 60 °C for 10 minutes before addition of the polythiol cross-linker. Stock solutions (100 mg/mL in dioxane) of cross-linkers were prepared and added to preassembled nanoparticle solution to synthesise the following; pentaerythritol tetrakis(3-mercaptopropionate (PTM), was used as a cross-linker to synthesise **NP$_{As\text{-}S4}$** (12.4 mg, 123 μL of cross-linker solution, 7.5 eq with respect to **P1**) and to synthesis **NP$_{As\text{-}S4/2}$** (6.18 mg, 61.8 μL of cross-linker solution, 3.75 eq with respect to **P1**); trimethylolpropane tris(3-mercaptopropionate) (TTM) was used as a cross-linker to synthesise **NP$_{As\text{-}S3}$** (13.5 mg, 135 μL of cross-linker solution, 10 eq with respect to **P1**) and to synthesis **NP$_{As\text{-}S3/2}$** (6.7 mg, 67.3 μL of cross-linker solution, 5 eq with respect to **P1**); hexa(ethylene glycol) dithiol (HDT) was used as a cross-linker to synthesise **NP$_{As\text{-}S2}$** (11.5 mg, 115 μL of cross-linker solution, 15 eq with respect to **P1**). The cross-linking reaction was left for 2 hours at 60 °C. The resulting solution was dialysed (nMWCO 3.5 KDa) for 3 days with deionised water, changing the water twice a day to remove electrolytes and dioxane. The cross-linked particles were isolated by lyophilisation to obtain white solid (yielded approximately between 95 - 99%) and were readily dispersed in H_2O.

General procedure for particle stability and disassembly.

Polymer nanoparticles (1 mg/mL), were dissolved separately in deionised water, glutathione (5 mM) and H_2O_2 (5 mM). The solutions were filtered through (450 μm nylon filters) into separate plastic cuvettes (with a lid) and incubated at 37 ^{0}C in water bath. Disassembly was monitored through the measurement of changes in particle size (D_h) as a function of time by DLS.

Atomic Force Microscopy (AFM)

AFM images were recorded on a Bruker Dimension Icon instrument operated in peak force tapping mode. The probes used were ScanAsyst silicon tips with a resonance frequency of 70 kHz and a spring constant of 0.4 N/m. Samples were prepared by drop casting 5 μl of a 1 mg/mL aqueous nanoparticle solution onto a freshly cleaved sheet of mica, left to stand for 30 seconds and then dried under a stream of Nitrogen.

Transmission Electron Microscopy (TEM)

Samples were prepared by placing a 400 mesh carbon coated Formvar copper grid onto a 20 μL droplet of aqueous nanoparticles (1 mg/mL) in a petri dish, leaving it for 10 minutes before drawing off the solution. The grid was then stained by placing onto a 20 μl droplet of aqueous solution of uranyl acetate (0.2 wt%), leaving it for 10 minutes before drawing off excess liquid and allowed to air-dry overnight. TEM images were acquired using a JEOL 2100 transmission electron microscope operating at a 200 kV accelerating voltage. Images were captured using Digital Micrograph® and analyzed with ImageJ.

Cell viability

Cell viability was assessed against MDA-231 (human breast adenocarcinoma) cell lines. Cells were seeded into a 96-well plate, (1.5 x 10^4 cells per well), cultured in basal medium DMEM

(Dublecco's Modified Eagle Medium) with 10% foetal bovine serum and allowed to grow for 24 hours. The medium was then replaced with fresh media contain As-functional nanoparticles (0.313, 0.625, 1.25, 2.50, 5.00 mg/mL) prepared from parent solutions of As-functional nanoparticles in media (5 mg/mL). Cells were further incubated for 24 hours. The medium was replaced with fresh medium containing a solution of XTT (0.2 mg/mL) and *N*-methyl dibenzopyrazine methyl sulphate (250 μM) and incubated for 16 hours. Cells were then transferred to a plate reader and absorbance at 450 and 650 nm was assessed.

RESULTS AND DISCUSSION

In previous work, block copolymeric arsenicals were synthesised by aqueous SET-LRP and were subsequently shown to undergo simultaneous self-assembly and reductive cross-linking (As-As) at elevated temperature in a reductive environment (H_3PO_2/KI).[38] Though aqueous SET-LRP is an ideal system for the polymerization of hydrophilic acrylamides and acrylates,[49] hydrolysis of the ω-bromine end group[50] can prove to be a limitation, and the use of relatively high concentrations of copper can add additional processing and purification steps. Having previously used RAFT polymerization for the homopolymerization of an organic arsenical acrylamide monomer (*N*-(4-(2,2,3,3,7,7,8,8-octamethyl-1,4,6,9-tetraoxa-5λ^5-arsaspiro[4.4]non-5-yl)-phenyl-2-propenamide; AsAm(pin)2)[46] and considering the advantages, most notably greater monomer scope, RAFT was employed here to synthesise thermoresponsive block copolymeric arsenicals for the first time, expanding their utility and versatility in polymer synthesis.

To investigate the effect of cross-linking using polythiol reagents on the formation and stability of polymeric arsenical nanoparticles, two polymer compositions incorporating the arsenic monomer into either the core-forming block (**P1**) or corona-forming block (**P2**) were targeted. The targeted composition of **P1** ($PEGA_{20}$-*b*-[$NIPAm_{70}$-*co*-$AsAm_{10}$]) was selected based on our

previous work where these thermoresponsive block copolymeric arsenicals were capable of forming stable nanoparticles via the reductive coupling method.[38] Likewise, the targeted composition of **P2** ([$PEGA_{15}$-*co*-$AsAm_5$]-*b*-$NIPAm_{80}$) was selected based on our previous work. This polymer did not form stable nanoparticles under reductive coupling but was investigated here to determine if the structures could be stabilised using potentially more robust polythiol cross-linkers.

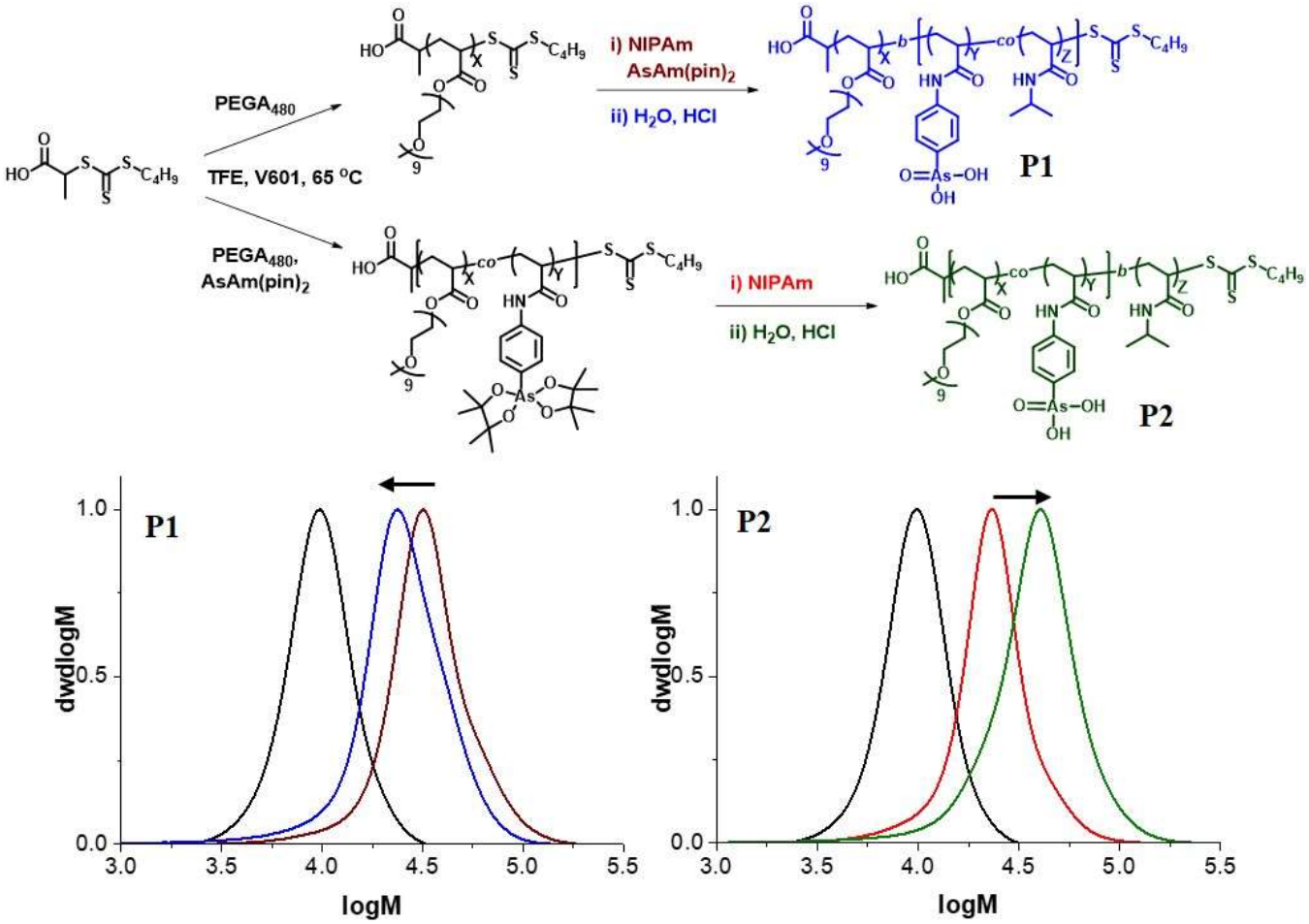

Figure 1: Scheme for the synthesis thermoresponsive block copolymeric arsenicals **P1 (**$PEGA_{22}$-*b*-[$NIPAm_{106}$-*co*-$AsAm_{15}$]) and **P2 (**[$PEGA_{17.5}$-*co*-$AsAm_{5.5}$]-*b*-$NIPAm_{97}$) by RAFT (top). SEC (DMF) of **P1** and **P2** showing: first block (black), chain extension (**P1p**, claret; **P2p**, red), after pinacol hydrolysis (**P1**, blue; **P2**, green) (bottom). See Table 1 for molecular weight data.

For the synthesis of **P1** ($PEGA_{20}$-*b*-[$NIPAm_{70}$-*co*-$AsAm_{10}$]), the polymerisation of the $PEGA_{480}$ corona-forming block gave good control ($M_{n,th}$ = 10800 $gmol^{-1}$, $M_{n,SEC}$ = 8900 $gmol^{-1}$, $Đ$ = 1.16) using 2-((butylthio)-carbonothioyl) thio propanoic acid (PABTC) as the RAFT agent. An initial monomer concentration ($PEGA_{480}$) of 1 M and initiator (V601) concentration of 9 x 10^{-4} M ($[CTA]_0/[I]_0$ = 50) led to near quantitative conversion (98%) at 65 °C after 24 hours. The conversion and degree of polymerization (DP_n) was determined by ^1H NMR (Figure S1) from the integral of the vinyl proton at 5.85 ppm and -CH_3 of the Z-group belonging to the PABTC (δ = 0.91 ppm). Chain extension using $AsAm(pin)_2$ and NIPAm with a combined monomer concentration of 3 M, initiator concentration of 1 x 10^{-3} M and $[MacroCTA]_0/[I]_0$ = 16, reached full conversion with respect to both monomers after 24 hours. Incorporation of $AsAm(pin_2)$ was verified and quantified by ^1H NMR through integration of the aromatic signal at 7.68 ppm furnishing the pinacol-protected polymer **P1p** with a final composition $PEGA_{22}$-*b*-[$NIPAm_{106}$-*co*-$AsAm(pin_2)_{15}$]. The block copolymerisation was also successfully demonstrated by SEC analysis showing a shift to a higher molecular weight ($M_{n,th}$ = 29600 $gmol^{-1}$, $M_{n,SEC}$ = 29300 $gmol^{-1}$, $Đ$ = 1.27) (Figure 1, Table 1).

An identical approach was followed for the synthesis of **P2** ([$PEGA_{15}$-*co*-$AsAm_5$]-*b*-$NIPAm_{80}$). A combined initial monomer concentration of 1 M for the PEGA and $AsAm(pin)_2$ monomers with PABTC and V601 (9 x 10^{-4} M) ($[CTA]_0/[I]_0$ = 39) gave quantitative conversion (99 %). The aromatic signal corresponding to the $AsAm(pin_2)$ monomer at 7.68 ppm was used to determine the proportion of $AsAm(pin_2)$ in the initial block (Figure S2). The aromatic peak at 7.80-7.50 ppm, was then used as a reference for subsequent chain extension to determine the [NIPAm]/[macroCTA] and a targeted DP_n = 80. The chain extension with NIPAm and $[MacroCTA]_0/[I]_0$ = 16 proceeded with quantitative monomer conversion furnishing the pinacol-

protected polymer **P2p** with a composition of [$PEGA_{17.5}$-*co*-$AsAm(pin_2)_{5.5}$]-*b*-$NIPAm_{97}$. Successful chain extension was further demonstrated by the SEC analysis ($M_{n,th}$ = 22100 $gmol^{-1}$, $M_{n,SEC}$ = 20500 $gmol^{-1}$, $Đ$ = 1.24) (Figure 1, Table 1).

To obtained the reactive block copolymeric arsenicals **P1** and **P2**, the pinacol groups of the $AsAm(pin_2)$ were removed by dialysis against 0.1 M HCl and de-ionized water to obtain the arsenic acid (AsAm, As(V))) functional pendent groups. Removal of the pinacol group from **P1p** and **P2p** to furnish **P1** and **P2** respectively was confirmed by ^{1}H NMR with disappearance of the pinacol -CH_3 signals at 1.27 and 1.00 ppm (Figure S3). In the case of **P1**, SEC revealed an expected decrease in $M_{n,th}$ resulting from loss of the pinacol groups ($M_{n,th}$ = 27100 $gmol^{-1}$, $M_{n,SEC}$ = 20800 $gmol^{-1}$, $Đ$ = 1.35). Interestingly, the deprotection of **P2p** to furnish **P2** resulted in a higher apparent molecular weight ($M_{n,th}$ = 21200 $gmol^{-1}$, $M_{n,SEC}$ = 30500 $gmol^{-1}$, $Đ$ = 1.35) (Figure 1, Table 1). This phenomenon was consistently observed in repeated syntheses of **P2** and in the synthesis of related scaffolds where the mole fraction of AsAm incorporated into the corona-forming PEGA block was varied (unpublished). This suggests that incorporation of AsAm into the corona-forming block has greater influence on the hydrodynamic volume of the copolymeric arsenicals than when AsAm is incorporated into the core-forming block.

Table 1. Arsenic functional block copolymers synthesised by RAFT.

	Polymer Composition	**Polymerisation mixture (P1p, P2p)**				**After deprotection**		
		Conv.[a]	$M_{n,th}$[b] **(g mol^{-1})**	$M_{n,SEC}$[c] **(g mol^{-1})**	$Đ$[c]	$M_{n,th}$[b] **(g mol^{-1})**	$M_{n,SEC}$[c] **(g mol^{-1})**	$Đ$[c]
P1	$P[PEGA_{22}]$	98 %	10800	8900	1.16			
	$P[PEGA_{22}$ -*b*-$(NIPAm_{106}$-*co*-$AsAm_{15})]$	> 99 %	29600	29300	1.27	26900	20800	1.35

P2	P[PEGA$_{17.5}$-*co*-AsAm$_{5.5}$]	98.5 %	11100	9000	1.15			
	P[(PEGA$_{17.5}$-*co*-AsAm$_{5.5}$)-*b*-NIPAm$_{97}$]	> 99 %	22100	20500	1.24	21100	30500	1.40

[a] ^{1}H NMR, $CDCl_3$; [b] Calculated using Eq 2, SI; [c] SEC, DMF

Prior to investigating the effect of polythiol cross-linking, the thermoresponsive behaviour and propensity for self-assembly of each copolymer was confirmed by variable temperature dynamic light scattering (DLS, 25-60 °C) in aqueous solutions (1 mg/mL). When the AsAm units were incorporated into the core-forming NIPAm block (**P1**), self-assembly occurred at T = 50 °C (D_h = 33 nm), and the nanoparticles contracted further with increasing temperature (D_h = 21 nm at T = 60 °C) (Figure 2). With the AsAm units incorporated in the corona forming PEGA block (**P2**), self-assembly occurred at lower temperatures (T = 40 °C, D_h = 21 nm), with contraction again observed with increasing temperature (D_h = 15 nm, at 60 °C) (Figure 2), forming smaller aggregates across the temperature range compared to **P1**.

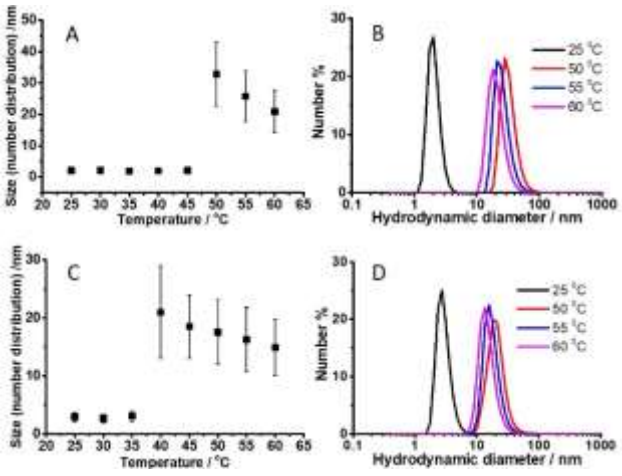

Figure 2. Variable temperature DLS analysis of thermally induced self-assembly of **P1** (A and B) and **P2** (C and D) between 25 – 60 °C, in aqueous solution (1 mg/mL).

One of the benefits of cross-linking thermoresponsive self-assembled polymers is being able to follow the success of cross-linking using DLS by returning the temperature back to that which the polymers would otherwise dissemble to unimer's without successful stabilisation. This

has previously been exemplified with nanostructures formed during polymerization induced thermal self-assembly (PITSA) of NIPAm, whereby covalent cross-linking at elevated temperatures results in retention of the nanostructures at ambient temperature.[51] The reactivity of arsenic offers a number of potential cross-linking strategies. In our previous work,[38] the simplest approach to cross-linking thermoresponsive block copolymeric arsenicals by simultaneous self-assembly and reductive coupling, resulting in the formation of As-As bonds in the form of $As(I)_n$ homocycles, was sufficient to stabilise core-functional copolymers, but not corona-functional copolymers. Consistent with this work **P2** was not stabilised by reductive coupling, whilst **P1** was successfully cross-linked to yield stable polymer nanoparticles ($\mathbf{NP_{As(I)}}$), as confirmed by DLS (D_h = 29 nm, Figure S4B), static light scattering (SLS, N_{agg} = 23, Figure S4E, S4F, Table 2), transmission electron microscopy (TEM, Figure S4C) and atomic force microscopy (AFM, Figure S4D).

The lability of the As-As bonds to hydrolysis and oxidation coupled with the high affinity of trivalent arsenic As(III) for thiol groups,[44, 52] inspired investigation of polythiol reagents as cross-linkers of thermally self-assembled polymers, **P1** and **P2**, through the formation of As-S bonds (Scheme 1). Although As(III) readily reacts with thiols to form As-S covalent bonds, pentavalent arsenic (As(V)) must first undergo reduction to As(III). This can be achieved via addition of excess thiol, with 2 equivalents required for reduction and a further 2 equivalents for bonding.[46, 53] In the context of this work, it was hypothesised that this would limit the cross-linking efficiency by diminishing the number of reactive thiol groups due to their oxidation (during the initial reduction process) to disulfides. Alternatively, non-thiol reducing agents could be considered to achieve *in-situ* reduction prior to addition of the polythiol cross-linkers. With this in mind the reductive conditions reported previously (H_3PO_2, KI, 60 °C) were adopted to

simultaneously afford self-assembly and initiate reduction of As(V) to As(III). It was proposed that the introduction of polythiol cross-linkers would pull the redox equilibrium towards the thiol cross-linked As(III) state, due to the formation of more enthalpically favoured As-S bonds. This hypothesis was verified by heating *p*-arsanilic acid under reductive conditions for 10 minutes prior to addition of a monothiol reagent (thiogylcerol, 2 eq), which resulted in the trapping of the As(III)-*bis*-thiogycerol adduct of *p*-arsanilic acid (Figure S5).

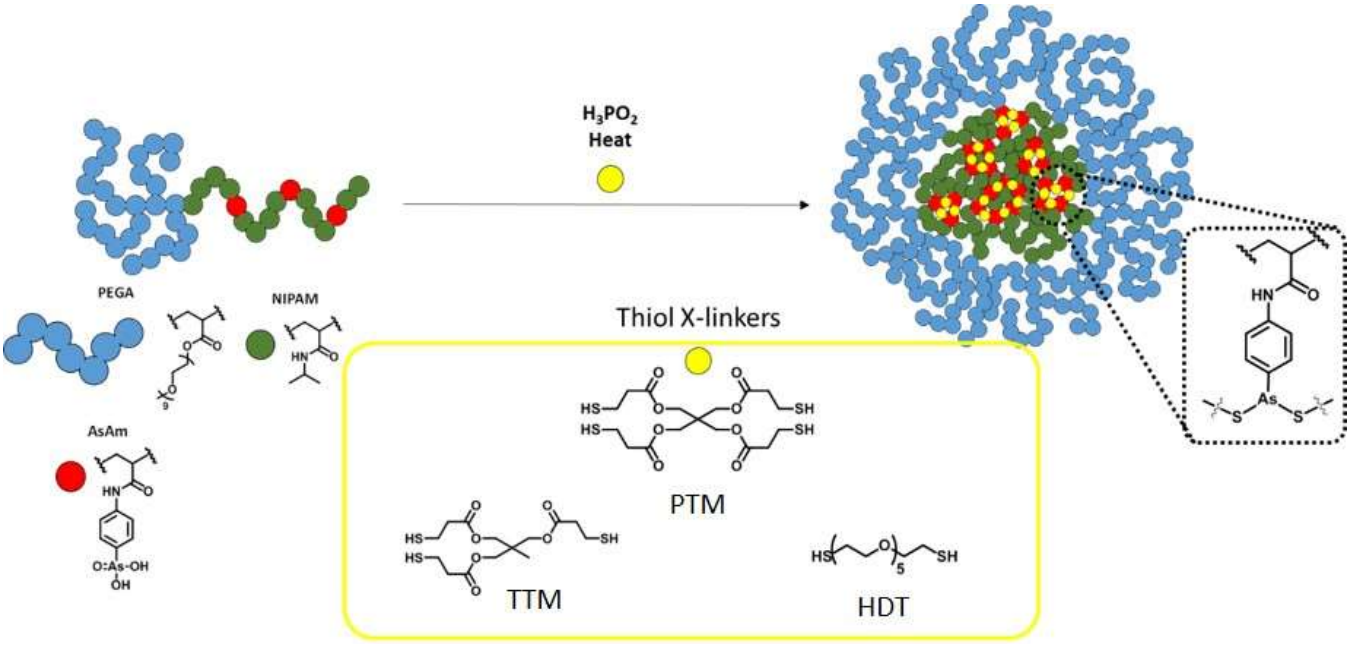

Scheme 1. Schematic representation of the proposed simultaneous self-assembly of and cross-linking of **P1** via polythiol reagents.

Pentaerythritol tetrakis(3-mercaptopropionate), (PTM), trimethylolpropane tris(3-mercaptopropionate) (TTM) and hexa(ethylene glycol) dithiol (HDT) were identified as potential tetra- tri- and di-functional cross-linkers with similar interatomic distances between each thiol group (Scheme 1). As the pendant As(III) groups can form two bonds to thiols, and to investigate the effect of the thiol valency of the cross-linkers, the stoichiometry of cross-linker was initially set so that [SH]/[As] = 2. For example, **P2** [$PEGA_{17.5}$-*co*-$AsAm_{5.5}$]-*b*-$NIPAm_{97}$, which does not

form stable nanoparticles when subjected to reductive conditions alone, was initially reacted with tetra-functional PTM (2.75 eq *i.e.* 11 eq [SH] w.r.t. [As]) in an attempt to stabilise the resulting nanoparticles. However, the formation of stable As-S cross-linked nanoparticles was not observed, with DLS analysis at room temperature confirming the presence of only unimers (Figure S6). This is attributed to the relatively low functional density of the As-groups in the corona which is also naturally more diffuse than the core, thus limiting the proximity of As(III) groups during the cross-linking process.

In contrast, when **P1** ($PEGA_{22}$-*b*-[$NIPAm_{106}$-*co*-$AsAm(pin_2)_{15}$]) was heated and subjected to reductive conditions, addition of PTM (7.5 eq) furnished stable nanoparticles (**$NP_{As\text{-}S4}$**), as observed by DLS (D_h = 29 nm, PDI = 0.06) measured at room temperature (Figure 3A) and TEM (Figure 3B). Cross-linking through the functional pendent As-groups was confirmed by IR with changes in the region between 1000 – 700 cm^{-1} (Figure S7). Specifically, the decrease in intensity of the signal at 750 cm^{-1} and the appearance of the signal at 810 cm^{-1} are consistent with reduction and thiol substitution as reported in previous work.[46] Static light scattering (SLS) was used to determine the absolute molecular weight ($M_{w,NP}$) from the Zimm plot and therefore the number of polymer chains per particle (Figure 3C, see SI for details). Interestingly, **$NP_{As\text{-}S4}$** was estimated to have an aggregation number (N_{agg}) of 278 chains per particle (at infinite dilution), which was considerably higher than the As-As cross-linked nanoparticles (**$NP_{As(I)}$**, Table 2). In previous work, the aqueous stability of **$NP_{As(I)}$** was shown to depend upon the mole fraction of AsAm present in the initial copolymer scaffolds.[38] In this investigation, the copolymers have a similar AsAm mole fraction to those that disassembled at t > 48 hrs in the previous study. It is therefore proposed that the differences in N_{agg} arise due to partial hydrolysis and disassembly of the aggregates during dialysis of **$NP_{As(I)}$**, which qualitatively reflects the relative stability of the As-S and As-As cross-

linking in aqueous solution. The molecular weight of the nanoparticles decreased with concentration, indicative of inter-particle interactions and inter-particle crosslinking at higher concentration (Figure 3D). This was supported by the ratio of the radius of gyration and radius of hydration ($\rho = R_g / R_h$) which can provide topological information, with $\rho = 0.778$ for a compact hard sphere, and 2.36 for a stiff rod.[54, 55] A ρ value of 1.39 was calculated for **NP$_{As\text{-}S4}$** at 1 mg/mL, which increased to 2.04 at higher concentration (4 mg/mL), indicating a change in topology, deviating further from spherical geometry as a result of inter-nanoparticle clustering. The proposed inter-nanoparticle interaction was also observed by AFM, which indicates clustering of the particles (Figure 3E, 3F).

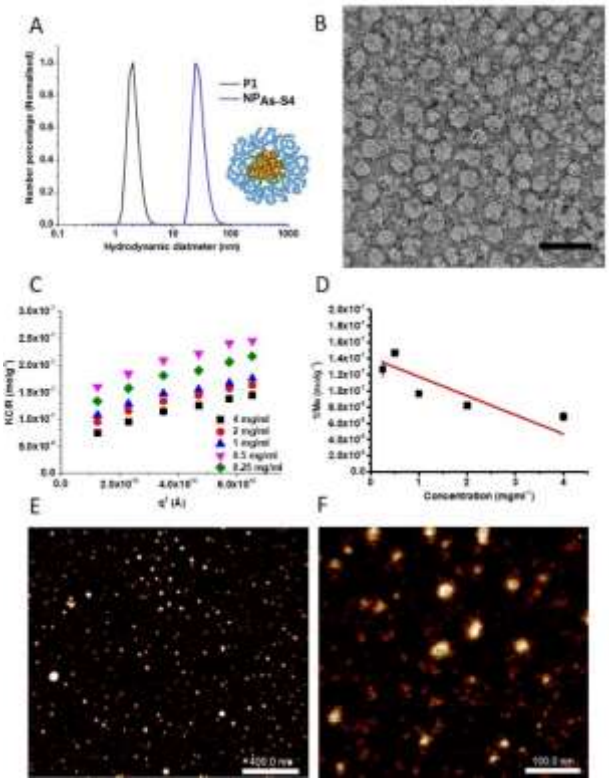

Figure 3. A) Particle size distribution (DLS) of **P1** (black) and **NP$_{As\text{-}S4}$** (blue); B) TEM image of **NP$_{As\text{-}S4}$** (scale bar = 100 nm); C) Zimm Plot for **NP$_{As\text{-}S4}$** showing the evolution of KC/R as a function of q^2 in aqueous solution from 0.25 – 4 mg/mL; D) Plot of the inverse of $M_{w,NP}$ of **NP$_{As\text{-}}$**

$_{S4}$ as a function of concentration (see SI for details); E) AFM image of **NP$_{As\text{-}S4}$** (scale bar = 400 nm); F) AFM image of **NP$_{As\text{-}S4}$** (scale bar = 100 nm).

To synthesize nanoparticles that were less densely cross-linked, the amount of cross-linker was reduced to half the stoichiometry ([SH]/[As] = 1, *i.e.* 3.75 eq PTM w.r.t. **P1**). The resulting nanoparticles (**NP$_{As\text{-}S4/2}$**) were successfully prepared and stable at room temperature (D_h = 23 nm, PDI = 0.11, Figure 4A). Reducing the stoichiometry resulted in a decrease in $M_{w,NP}$ and N_{agg} according to SLS analysis (Table 2), which also indicated that $M_{w,NP}$ was largely independent of concentration (Figure S8). A ρ value of 1.13 was obtained which was lower **NP$_{As\text{-}S4}$** (1.39 - 2.04, Table 2) across the concentration range, indicating that **NP$_{As\text{-}S4/2}$** exhibited a more spherical topology. This was confirmed by AFM which revealed limited nanoparticle clustering (Figure 4B).

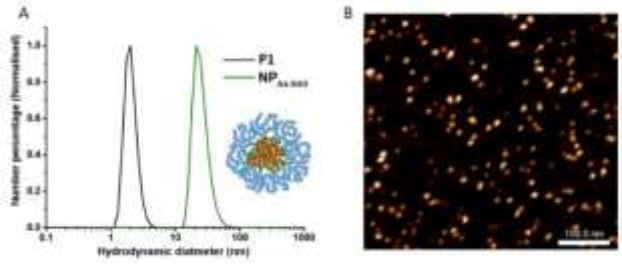

Figure 4. A) Particle size distribution (DLS) of **P1** (black) and **NP$_{As\text{-}S4/2}$** (green); B) AFM image of **NP$_{As\text{-}S4/2}$** (scale bar = 100 nm).

Based on their respective bond lengths, As-S[56] bonds are more stable than As-As[57] bonds in organic arsenicals. However, the As-S bonding can be dynamic in the presence of exchangeable thiols.[47] The stability and responsivity of **NP$_{As\text{-}S4}$** and **NP$_{As\text{-}S4/2}$** to glutathione (5 mM, 37 °C) was therefore investigated. Both sets of nanoparticles remained intact, even after one week, as observed by no change in the hydrodynamic size by DLS analysis (Figure 5A, 5B). This represents a marked increase in stability to GSH compared to **NP$_{As(I)}$** which disassembled within 3 hours (Figure 5C).

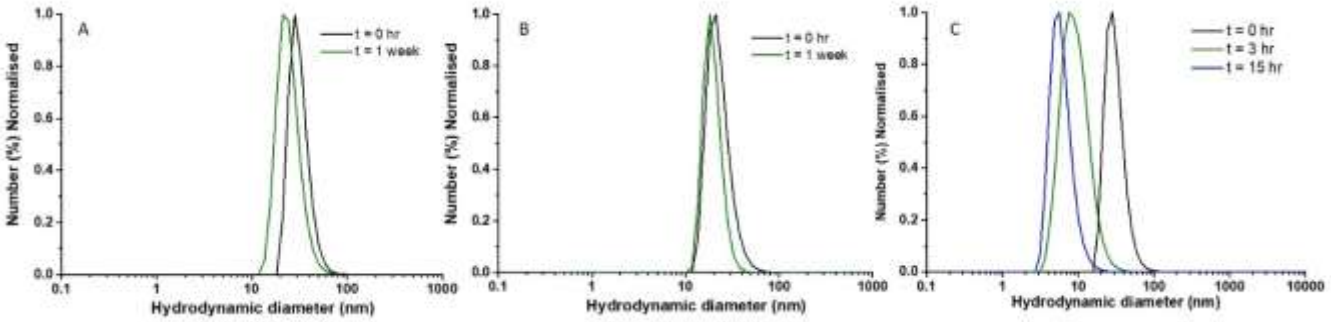

Figure 5. Particle size distribution curves (DLS) for A) $\mathbf{NP_{As\text{-}S4}}$; B) $\mathbf{NP_{As\text{-}S4/2}}$; C) $\mathbf{NP_{As(I)}}$ (1 mg/mL) as a function of time in in aqueous GSH (5 mM).

An alternative approach to tuning the cross-linking is through the thiol valency in the polythiol cross-linkers. When **P1** was subjected to reductive conditions and tri-functional (TTM; 10 eq w.r.t. **P1**) and di-functional (HDT; 15 eq w.r.t. **P1**) cross-linkers were added ([SH]/[As] = 2) to independent batches, stable nanoparticles $\mathbf{NP_{As\text{-}S3}}$ (D_h = 25, PDI = 0.09, Figure S9A) and $\mathbf{NP_{As\text{-}S2}}$ (D_h = 19 nm, PDI = 0.11, Figure S10A) were retained at room temperature. According to SLS analysis $\mathbf{NP_{As\text{-}S3}}$ were similar to $\mathbf{NP_{As\text{-}S4}}$ exhibiting a slight decrease in $M_{w,NP}$ and N_{agg} (N_{agg} = 204, Table 2), of which $M_{w,NP}$ was shown to be dependent upon concentration (Figure S9C, S9D) resulting in ρ values from 1.28 (1 mg/mL) to 2.48 (4 mg/mL). Conversely, for $\mathbf{NP_{As\text{-}S2}}$ both $M_{w,NP}$ and N_{agg} were found to be significantly lower (N_{agg} = 26, Figure S10C, S10D) and the ρ values (1.60 - 1.64), although higher than anticipated, were similar across the concentration range (Table 2). As the ρ values suggest, inter-particle clustering was evident by AFM of $\mathbf{NP_{As\text{-}S3}}$ (Figure S9B) and $\mathbf{NP_{As\text{-}S2}}$ (Figure S10B). Reducing the stoichiometry ([SH]/[As] = 1) during the TTM and HDT cross-linking had a profound effect. The nanoparticles prepared using TTM ($\mathbf{NP_{As\text{-}S3/2}}$) exhibit the same trend as observed for $\mathbf{NP_{As\text{-}S4/2}}$, *i.e.* lower $M_{w,NP}$, N_{agg} and less particle clustering compared to $\mathbf{NP_{As\text{-}S3}}$ (Figure S11). Conversely, although those prepared using HDT ($\mathbf{NP_{As\text{-}S2/2}}$) were initially stable at ambient temperature, purification by dialysis to remove any excess reagents resulted in

disassembly of **NP$_{As\text{-}S2/2}$** (Figure S10A).

Table 2. Light scattering analysis (DLS and SLS) of the As-nanoparticles. DLS was measured in aqueous solution (1 mg/mL). The ratio R_g/R_h at 4 mg/mL and 1 mg/mL is displayed for comparison.

		SLS				DLS	
NP	dn/dC[a] (mL/g)	$M_{W,NP}$[b] (g/mol)	N_{agg}[c]	R_g/R_h[d] (4 mg/mL)	R_g/R_h[d] (1 mg/mL)	D_h (nm)	PDI[e]
NP$_{S4}$	0.137	7.5×10^6	277	2.04	1.39	29	0.06
NP$_{As\text{-}S4/2}$	0.189	1.4×10^6	52	1.13	0.90	23	0.11
NP$_{As\text{-}S3}$	0.133	5.5×10^6	203	2.48	1.28	25	0.09
NP$_{As\text{-}S3/2}$	0.190	7.2×10^5	27	1.08	1.11	21	0.11
NP$_{As\text{-}S2}$	0.174	7.0×10^5	26	1.64	1.60	19	0.11
NP$_{As\text{-}S2/2}$	-	-	-	-	-	5.4	0.07
NP$_{As(I)}$	0.164	6.3×10^5	23	3.42	1.27	29	0.12

[a] Determined by measuring the refractive index over a range of concentrations (1.33, 0.66, 0.33, 0.167 mg/mL); [b] $M_{w,NP}$ was determined using Eq 3-5 (SI); [c] $N_{agg} = M_{w,NP}/M_{n,th}$; [d] R_g is the gradient of Zimm plots and R_h was determined as the size measured from the scattering angle at 90 ° from SLS; Measured using Eq 1 (SI).

The trends in particle structure were reflected in the nanoparticle stability and initial responsivity to thiol exchange. Similar to **NP$_{As\text{-}S4}$** and **NP$_{As\text{-}S4/2}$**, both **NP$_{As\text{-}S3}$** and **NP$_{As\text{-}S3/2}$** remained intact even after a week in the presence of GSH (5 mM, 37 °C, Figure S12A, S12B). However, **NP$_{As\text{-}S2}$** was found to be less stable than **NP$_{As\text{-}S3}$** and **NP$_{As\text{-}S4}$**, disassembling between 48 to 72 hours in the presence of GSH (5 mM, 37 °C, Figure S12C). This is attributed to the tetra- (PTM) and tri-thiol (TTM) cross-linkers affording greater cross-linking density and imposing a higher entropic barrier to thiol exchange with monothiol reagents such as GSH compared to the di-thiol (HDT) analogue.

The dynamic redox chemistry of arsenic is a distinctive characteristic of organic and polymeric arsenicals that lends itself to application in the development of redox responsive (bio)nanomaterials. It is known that As(III) can be readily oxidise to As(V) by reactive oxygen species (ROS) such as hydrogen peroxide (H_2O_2).[58] Suzuki *et al* have treated blood and organ lysates from animal models (Hamsters and Rats) with H_2O_2 to liberate As(III) bound proteins as arsenates (As(V)) for arsenic biodistribution and metabolite assays.[59] Likewise, computational studies by Villamena *et al* suggests As(III) oxidation to As(V) by ROS species including hydrogen peroxide is exoergic, and highlight the possibility of arsenic cytotoxicity by GSH depletion due to the redox cycling events between GSH (As(V) reduction) and ROS (As(III) oxidation).[60]

Here, the responsivity of the As-S cross-linked nanoparticles to H_2O_2 was investigated with the proposed response to As-S bond cleavage and oxidation (As(III) to As(V)) monitored as a function of the particle size using DLS (Figure 6). The nanoparticles stabilised by As-S cross-linking (**$NP_{As\text{-}S4}$, $NP_{As\text{-}S4/2}$, $NP_{As\text{-}S3}$, $NP_{As\text{-}S3/2}$, $NP_{As\text{-}S2}$**) did not disassemble instantly, maintaining the hydrodynamic particle sizes over the first 3 hours. This is in contrast to the nanoparticles cross-linked by reductive coupling only (**$NP_{As(I)}$**), which fully disassembled within 1 hour after addition of H_2O_2 (5 mM, 37 °C, Figure S13). A trend was observed relating the nanoparticle stability to the structure of the polythiol cross-linkers and the cross-linking density. The stability of the particles decreased with decreasing thiol valency in the cross-linkers ([SH] : [As] = 2; **$NP_{As\text{-}S4}$ > $NP_{As\text{-}S3}$ > $NP_{As\text{-}S2}$**) with **$NP_{As\text{-}S4}$** (Figure 6B) undergoing disassembly over 44 hours and **$NP_{As\text{-}S3}$** (Figure 6C) and **$NP_{As\text{-}S2}$** (Figure 6D) disassembling over 18 hours and 6 hours respectively.

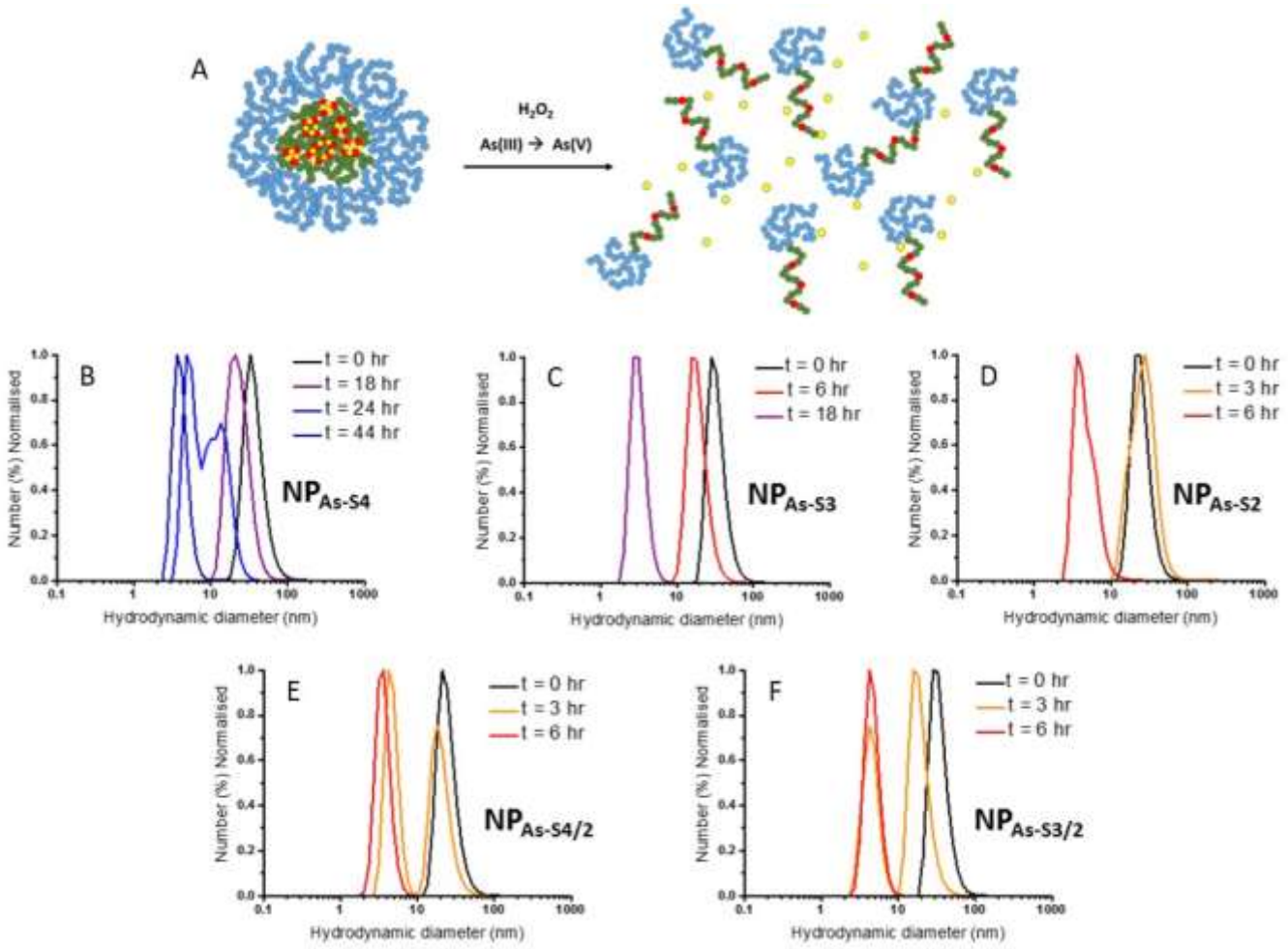

Figure 6. A) Schematic representation of the oxidative disassembly of the As-nanoparticles in the presence of H_2O_2; Particle size distribution curves (DLS) for B) $\mathbf{NP_{As\text{-}S4}}$; C) $\mathbf{NP_{As\text{-}S3}}$; D) $\mathbf{NP_{As\text{-}S2}}$; E) $\mathbf{NP_{As\text{-}S4/2}}$; F) $\mathbf{NP_{As\text{-}S3/2}}$; as a function of time in in aqueous H_2O_2 (5 mM).

When the cross-linking density was reduced ([SH] : [As] = 1; $\mathbf{NP_{As\text{-}S4/2}}$ and $\mathbf{NP_{As\text{-}S3/2}}$) the stability was reduced further with the onset of disassembly occurring within 3 hours (Figure 6E, 6F). This trend can be attributed to the thiol valency in the cross-linkers *i.e.* increasing valency PTM > TTM > HDT increases the likelihood of inter-chain As-S bonds forming, constituting cross-linking, which have to be broken under the oxidative conditions. Intra-chain As-S bonding is also possible, and this will have a more detrimental effect when di-thiol HDT is employed ($\mathbf{NP_{As\text{-}S2}}$) as a single intra-chain reaction will consume both the thiol groups at the expense of cross-linking

However, when PTM and TTM are employed (**NP**$_{\text{As-S4}}$ and **NP**$_{\text{As-S3}}$), there are latent thiol groups available for cross-linking should an intra-chain reaction occur. These results demonstrate for the first time that nanoparticles compromised of polymeric arsenicals, cross-linked via As-S bonds have tuneable responsivity to H_2O_2, which is an attractive stimulus for drug delivery, particularly as a responsive linker for peroxisomes targeted delivery is also particularly interesting, especially in intracellular infections.[61] Furthermore, H_2O_2 is indigenously produced inside cells for natural cellular processing[62] and its concentration is increased in environments of oxidative stress which occurs in response to inflammation associated with a number of disease states including cancer and atherosclerosis and cystic fibrosis.

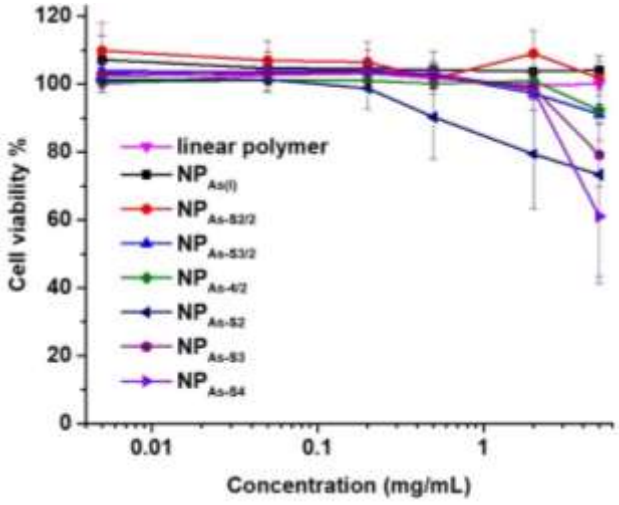

Figure 7. *In vitro* cell viability of polymer **P1** and the As-nanoparticles (XTT viability assay using MDA cell line).

Finally, to dispel concerns regarding the toxicity of organic and polymeric arsenicals, which are known to be less toxic than inorganic counterparts, *in vitro* toxicity of the polymeric arsenical **P1** and the resulting nanoparticles was determined using a standard XTT assay with a human breast adenocarcinoma cell line (MDA-231). Using an identical protocol, polymeric arsenical scaffolds have been shown to be non-toxic between 2 – 20 μM against MDA-231, whilst

nanoparticles derived from thermoresponsive block copolymeric arsenicals, similar to those reported here but consisting of As-As cross-linking, were also non-toxic up to 2 mg/mL against a Prostate cancer cell line (PC3). In this work **P1** was non-toxic up to 5 mg/mL and the nanoparticles were non-toxic up to 2 mg/mL with the exception of the $\mathbf{NP_{As\text{-}S2}}$ which showed a decrease in cell viability at concentration > 0.2 mg/mL (Figure 7). This is attributed to the lower stability of $\mathbf{NP_{As\text{-}S2}}$ leading to an earlier onset of disassembly, with the products of the disassembly being responsible for the change in viability. The origin of the toxicity is not known at this stage but the released cross-linker is implicated considering that **P1** is non-toxic over the concentration range. Despite this result, and since it occurs at high concentration (from a clinical perspective), these results support the potential of using polymeric arsenicals as a platform for stimuli responsive drug delivery.

CONCLUSIONS

Thermoresponsive block copolymeric arsenicals comprised of $PEGA_{480}$ and NIPAm, with incorporation of organic arsenical acrylamide monomer ($AsAm(pin_2)$) into either the core-forming NIPAm block ($PEGA_{22}$-*b*-($NIPAm_{106}$-*co*-$AsAm(pin_2)_{15}$, **P1p**) or the corona-forming PEGA block ([$PEGA_{17.5}$-*co*-$AsAm(pin_2)_{5.5}$]-*b*-$NIPAm_{97}$, **P2p**), have been synthesised by RAFT for the first time. Removal of the pinacol groups of $AsAm(pin_2)$ furnished reactive As(V)-functional groups and the resulting polymers (**P1**/**P2**) formed nanoparticles at elevated temperatures. The reactive As(V)-functional groups were targeted for cross-linking under reductive conditions (H_3PO_2, KI, 60 °C) in the presence of polythiol reagents (PTM, TTM, HDT) exploiting the high affinity of the As(III) for thiols and affording cross-linking through the formation of As(III)-S bonds. The corona-functional polymer **P2** was not able to be stabilised even in the presence of tetra-thiol cross-linker PTM and targeting 100% cross-linking ([SH] : [As] = 2). However, the core-functional

polymer **P1** formed stable nanoparticles in the presence of tetra- (PTM, $\mathbf{NP_{As\text{-}S4}}$), tri- (TTM, $\mathbf{NP_{As\text{-}S3}}$) and di-thiol (HDT, $\mathbf{NP_{As\text{-}S2}}$) cross-linkers ([SH] : [As] = 2), which were more stable than analogous nanoparticles cross-linked by complete reductive coupling via As-As bond formation $\mathbf{NP_{As(I)}}$. Characterisation of the nanoparticles by SLS, AFM and TEM revealed that N_{agg} and R_g/R_h increased as a function of concentration for $\mathbf{NP_{As\text{-}S4}}$ and $\mathbf{NP_{As\text{-}S3}}$ which was manifest as changes in nanoparticle topology as a result of inter-particle interactions and aggregation. Conversely, $\mathbf{NP_{As\text{-}S2}}$ and nanoparticles prepared targeting 50% cross-linking ([SH] : [As] = 1; $\mathbf{NP_{As\text{-}S4/2}}$, $\mathbf{NP_{As\text{-}S3/2}}$) exhibited more spherical structures and showed little change in N_{agg} and R_g/R_h. With respect to stability and responsivity of these nanoparticles only $\mathbf{NP_{As\text{-}S2}}$ was shown to disassemble in the presence GSH (5 mM, 37 °C) which occurred over 72 hours. In contrast, a trend was observed pertaining to disassembly under conditions mimicking oxidative stress H_2O_2 (5 mM, 37 °C), whereby the stability of the particles followed the trend $\mathbf{NP_{As\text{-}S4}} > \mathbf{NP_{As\text{-}S3}} > \mathbf{NP_{As\text{-}S2}} > \mathbf{NP_{As\text{-}S4/2}} \approx \mathbf{NP_{As\text{-}S3/2}}$. To the best of our knowledge this is the first report in the literature that As-S bonding has been exploited to cross-link polymeric nanoparticles that are responsive to oxidative stress. The diverse chemistry and non-toxic nature of the polymeric arsenicals and nanoparticles demonstrated here and in our previous works, combined with the potential synergy with respect to biological activity, strengthens the case for broader acceptance and adoption of polymeric arsenicals as a functional and responsive platform for biomaterials science.

ASSOCIATED CONTENT

Supporting Information. Additional information regarding the materials and methods employed during this work are include in the supplementary information file associated with this manuscript and available free of charge form the ACS website.

Details of materials and instrumentation; equations employed for the calculation of PDI (DLS), $M_{n,th}$ (NMR), M_w (SLS); supporting figures for the synthesis of **P1** and **P2**; supporting figures for the formation and responsivity (to GSH) of nanoparticles $\mathbf{NP_{As(I)}}$, $\mathbf{NP_{As\text{-}S3}}$, $\mathbf{NP_{As\text{-}S2}}$, $\mathbf{NP_{As\text{-}S3/2}}$.

AUTHOR INFORMATION

Corresponding Author

*Paul Wilson; p.wilson.1@warwick.ac.uk

Funding Sources

Engineering and Physical Sciences Research Council (EPSRC); EP/F500378/1

Australian Research Council (ARC); CE140100036

Royal Society; WM130055

Leverhulme Trust; ECF/2015-075

ACKNOWLEDGMENT

The authors gratefully acknowledge financial support from Engineering and Physical Sciences Research Council (EPSRC) under grant EP/F500378/1 through the Molecular Organization and Assembly in Cells Doctoral Training Centre (MOAC-DTC). The authors also wish to acknowledge the facilities and personnel (T.P.D., S.P., P.W.) enabled by the Monash-Warwick Alliance. This work was carried out in conjunction with the Australian Research Council (ARC) Centre of Excellence in Convergent Bio-NanoScience and Technology (CE140100036). T.P.D. gratefully acknowledges support from the ARC in the form of an Australian Laureate Fellowship. S.P. acknowledges a Royal Society Wolfson Merit Award (WM130055). P.W. thanks the Leverhulme

Trust for the award of an Early Career Fellowship (ECF/2015-075). The authors would like to thank the Polymer Characterization and Microscopy Research Technology Platform for access and use of SEC, AFM and TEM facilities.

REFERENCES

1. Kim, J. K.; Yang, S. Y.; Lee, Y.; Kim, Y. Functional nanomaterials based on block copolymer self-assembly. *Prog. Polym. Sci.* **2010,** 35 (11), 1325-1349.
2. Mai, Y.; Eisenberg, A. Self-assembly of block copolymers. *Chem. Soc. Rev.* **2012,** 41 (18), 5969-5985.
3. Cabral, H.; Miyata, K.; Osada, K.; Kataoka, K. Block Copolymer Micelles in Nanomedicine Applications. *Chem. Rev.* **2018,** 118 (14), 6844-6892.
4. Zhang, S. Fabrication of novel biomaterials through molecular self-assembly. *Nat. Biotechnol.* **2003,** 21, 1171.
5. Park, C.; Yoon, J.; Thomas, E. L. Enabling nanotechnology with self assembled block copolymer patterns. *Polymer* **2003,** 44 (22), 6725-6760.
6. De Martino, M. T.; Abdelmohsen, L. K. E. A.; Rutjes, F. P. J. T.; van Hest, J. C. M. Nanoreactors for green catalysis. *Beilstein J. Org. Chem.* **2018,** 14, 716-733.
7. Hirao, A.; Goseki, R.; Ishizone, T. Advances in Living Anionic Polymerization: From Functional Monomers, Polymerization Systems, to Macromolecular Architectures. *Macromolecules* **2014,** 47 (6), 1883-1905.
8. Keddie, D. J. A guide to the synthesis of block copolymers using reversible-addition fragmentation chain transfer (RAFT) polymerization. *Chem. Soc. Rev.* **2014,** 43 (2), 496-505.
9. Nicolas, J.; Guillaneuf, Y.; Lefay, C.; Bertin, D.; Gigmes, D.; Charleux, B. Nitroxide-mediated polymerization. *Prog. Polym. Sci.* **2013,** 38 (1), 63-235.
10. Matyjaszewski, K. Advanced Materials by Atom Transfer Radical Polymerization. *Adv. Mater.* **2018,** 30 (23), 1706441.
11. Anastasaki, A.; Nikolaou, V.; Nurumbetov, G.; Wilson, P.; Kempe, K.; Quinn, J. F.; Davis, T. P.; Whittaker, M. R.; Haddleton, D. M. Cu(0)-Mediated Living Radical Polymerization: A Versatile Tool for Materials Synthesis. *Chem. Rev.* **2016,** 116 (3), 835-877.
12. Engelis, N. G.; Anastasaki, A.; Nurumbetov, G.; Truong, N. P.; Nikolaou, V.; Shegiwal, A.; Whittaker, M. R.; Davis, T. P.; Haddleton, D. M. Sequence-controlled methacrylic multiblock copolymers via sulfur-free RAFT emulsion polymerization. *Nat. Chem.* **2017,** 9 (2), 171-178.
13. Anastasaki, A.; Nikolaou, V.; McCaul, N. W.; Simula, A.; Godfrey, J.; Waldron, C.; Wilson, P.; Kempe, K.; Haddleton, D. M. Photoinduced Synthesis of α,ω-Telechelic Sequence-Controlled Multiblock Copolymers. *Macromolecules* **2015,** 48 (5), 1404-1411.
14. Aksakal, R.; Resmini, M.; Becer, C. R. Pentablock star shaped polymers in less than 90 minutes via aqueous SET-LRP. *Polym. Chem.* **2016,** 7 (1), 171-175.
15. Zhang, J.; Tanaka, J.; Gurnani, P.; Wilson, P.; Hartlieb, M.; Perrier, S. Self-assembly and disassembly of stimuli responsive tadpole-like single chain nanoparticles using a switchable hydrophilic/hydrophobic boronic acid cross-linker. *Polym. Chem.* **2017,** 8 (28), 4079-4087.
16. Jain, S.; Bates, F. S. On the origins of morphological complexity in block copolymer surfactants. *Science* **2003,** 300 (5618), 460-4.

17. Elsabahy, M.; Wooley, K. L. Design of polymeric nanoparticles for biomedical delivery applications. *Chem. Soc. Rev.* **2012,** 41 (7), 2545-2561.
18. Wilhelm, M.; Zhao, C. L.; Wang, Y.; Xu, R.; Winnik, M. A.; Mura, J. L.; Riess, G.; Croucher, M. D. Poly(styrene-ethylene oxide) block copolymer micelle formation in water: a fluorescence probe study. *Macromolecules* **1991,** 24 (5), 1033-1040.
19. Hsiao, M.-S.; Yusoff, S. F. M.; Winnik, M. A.; Manners, I. Crystallization-Driven Self-Assembly of Block Copolymers with a Short Crystallizable Core-Forming Segment: Controlling Micelle Morphology through the Influence of Molar Mass and Solvent Selectivity. *Macromolecules* **2014,** 47 (7), 2361-2372.
20. Sarett, S. M.; Werfel, T. A.; Chandra, I.; Jackson, M. A.; Kavanaugh, T. E.; Hattaway, M. E.; Giorgio, T. D.; Duvall, C. L. Hydrophobic interactions between polymeric carrier and palmitic acid-conjugated siRNA improve PEGylated polyplex stability and enhance in vivo pharmacokinetics and tumor gene silencing. *Biomaterials* **2016,** 97, 122-132.
21. Nakanishi, T.; Fukushima, S.; Okamoto, K.; Suzuki, M.; Matsumura, Y.; Yokoyama, M.; Okano, T.; Sakurai, Y.; Kataoka, K. Development of the polymer micelle carrier system for doxorubicin. *J. Controlled Release* **2001,** 74 (1-3), 295-302.
22. Harada, A.; Kataoka, K. Formation of Polyion Complex Micelles in an Aqueous Milieu from a Pair of Oppositely-Charged Block Copolymers with Poly(ethylene glycol) Segments. *Macromolecules* **1995,** 28 (15), 5294-5299.
23. Kim, S. H.; Tan, J. P. K.; Nederberg, F.; Fukushima, K.; Colson, J.; Yang, C.; Nelson, A.; Yang, Y.-Y.; Hedrick, J. L. Hydrogen bonding-enhanced micelle assemblies for drug delivery. *Biomaterials* **2010,** 31 (31), 8063-8071.
24. Jeong, Y.-H.; Shin, H.-W.; Kwon, J.-Y.; Lee, S.-M. Cisplatin-Encapsulated Polymeric Nanoparticles with Molecular Geometry-Regulated Colloidal Properties and Controlled Drug Release. *ACS Appl. Mater. Interfaces* **2018,** 10 (28), 23617-23629.
25. Talelli, M.; Barz, M.; Rijcken, C. J.; Kiessling, F.; Hennink, W. E.; Lammers, T. Core-Crosslinked Polymeric Micelles: Principles, Preparation, Biomedical Applications and Clinical Translation. *Nano Today* **2015,** 10 (1), 93-117.
26. Wooley, K. L. Shell crosslinked polymer assemblies: Nanoscale constructs inspired from biological systems. *J. Polym. Sci. Part A: Polym. Chem.* **2000,** 38 (9), 1397-1407.
27. Xin, Y.; Yuan, J. Schiff's base as a stimuli-responsive linker in polymer chemistry. *Polym. Chem.* **2012,** 3 (11), 3045-3055.
28. Mukherjee, S.; Bapat, A. P.; Hill, M. R.; Sumerlin, B. S. Oximes as reversible links in polymer chemistry: dynamic macromolecular stars. *Polym. Chem.* **2014,** 5 (24), 6923-6931.
29. Shi, Y.; van Nostrum, C. F.; Hennink, W. E. Interfacially Hydrazone Cross-linked Thermosensitive Polymeric Micelles for Acid-Triggered Release of Paclitaxel. *ACS Biomater. Sci. Eng.* **2015,** 1 (6), 393-404.
30. Quinn, J. F.; Whittaker, M. R.; Davis, T. P. Glutathione responsive polymers and their application in drug delivery systems. *Polym. Chem.* **2017,** 8 (1), 97-126.
31. Brooks, W. L. A.; Sumerlin, B. S. Synthesis and Applications of Boronic Acid-Containing Polymers: From Materials to Medicine. *Chem. Rev.* **2016,** 116 (3), 1375-1397.
32. Xu, X.; Saw, P. E.; Tao, W.; Li, Y.; Ji, X.; Bhasin, S.; Liu, Y.; Ayyash, D.; Rasmussen, J.; Huo, M.; Shi, J.; Farokhzad, O. C. ROS-Responsive Polyprodrug Nanoparticles for Triggered Drug Delivery and Effective Cancer Therapy. *Adv. Mater.* **2017,** 29 (33), 1700141.
33. Roy, D.; Sumerlin, B. S. Glucose-Sensitivity of Boronic Acid Block Copolymers at Physiological pH. *ACS Macro Lett.* **2012,** 1 (5), 529-532.

34. Hu, J.; Zhang, G.; Liu, S. Enzyme-responsive polymeric assemblies, nanoparticles and hydrogels. *Chem. Soc. Rev.* **2012,** 41 (18), 5933-5949.
35. Fleige, E.; Quadir, M. A.; Haag, R. Stimuli-responsive polymeric nanocarriers for the controlled transport of active compounds: Concepts and applications. *Adv. Drug Delivery Rev.* **2012,** 64 (9), 866-884.
36. Adams, M. L.; Lavasanifar, A.; Kwon, G. S. Amphiphilic block copolymers for drug delivery. *J. Pharm. Sci.* **2003,** 92 (7), 1343-1355.
37. Lloyd, N. C.; Morgan, H. W.; Nicholson, B. K.; Ronimus, R. S. The Composition of Ehrlich's Salvarsan: Resolution of a Century-Old Debate. *Angew. Chem. Int. Ed.* **2005,** 44 (6), 941-944.
38. Tanaka, J.; Tani, S.; Peltier, R.; Pilkington, E. H.; Kerr, A.; Davis, T. P.; Wilson, P. Synthesis, aggregation and responsivity of block copolymers containing organic arsenicals. *Polym. Chem.* **2018,** 9 (13), 1551-1556.
39. Shen, S.; Li, X.-F.; Cullen, W. R.; Weinfeld, M.; Le, X. C. Arsenic Binding to Proteins. *Chem. Rev.* **2013,** 113 (10), 7769-7792.
40. Park, D.; Chiu, J.; Perrone, G. G.; Dilda, P. J.; Hogg, P. J. The tumour metabolism inhibitors GSAO and PENAO react with cysteines 57 and 257 of mitochondrial adenine nucleotide translocase. *Cancer Cell Int.* **2012,** 12 (1), 11.
41. Don, A. S.; Kisker, O.; Dilda, P.; Donoghue, N.; Zhao, X.; Decollogne, S.; Creighton, B.; Flynn, E.; Folkman, J.; Hogg, P. J. A peptide trivalent arsenical inhibits tumor angiogenesis by perturbing mitochondrial function in angiogenic endothelial cells. *Cancer Cell* **2003,** 3 (5), 497-509.
42. Dilda, P. J.; Decollogne, S.; Weerakoon, L.; Norris, M. D.; Haber, M.; Allen, J. D.; Hogg, P. J. Optimization of the Antitumor Efficacy of a Synthetic Mitochondrial Toxin by Increasing the Residence Time in the Cytosol. *J. Med. Chem.* **2009,** 52 (20), 6209-6216.
43. Dilda, P. J.; Hogg, P. J. Arsenical-based cancer drugs. *Cancer Treat. Rev.* **2007,** 33 (6), 542-564.
44. Spuches, A. M.; Kruszyna, H. G.; Rich, A. M.; Wilcox, D. E. Thermodynamics of the As(III)−Thiol Interaction: Arsenite and Monomethylarsenite Complexes with Glutathione, Dihydrolipoic Acid, and Other Thiol Ligands. *Inorg. Chem.* **2005,** 44 (8), 2964-2972.
45. Griffin, B. A.; Adams, S. R.; Tsien, R. Y. Specific Covalent Labeling of Recombinant Protein Molecules Inside Live Cells. *Science* **1998,** 281 (5374), 269-272.
46. Footman, C.; de Jongh, P. A. J. M.; Tanaka, J.; Peltier, R.; Kempe, K.; Davis, T. P.; Wilson, P. Thiol-reactive (co)polymer scaffolds comprising organic arsenical acrylamides. *Chem. Commun.* **2017,** 53 (60), 8447-8450.
47. Wilson, P.; Anastasaki, A.; Owen, M. R.; Kempe, K.; Haddleton, D. M.; Mann, S. K.; Johnston, A. P. R.; Quinn, J. F.; Whittaker, M. R.; Hogg, P. J.; Davis, T. P. Organic Arsenicals As Efficient and Highly Specific Linkers for Protein/Peptide–Polymer Conjugation. *J. Am. Chem. Soc.* **2015,** 137 (12), 4215-4222.
48. Noy, J.-M.; Lu, H.; Hogg, P. J.; Yang, J.-L.; Stenzel, M. Direct Polymerization of the Arsenic Drug PENAO to Obtain Nanoparticles with High Thiol-Reactivity and Anti-Cancer Efficiency. *Bioconjugate Chem.* **2018,** 29 (2), 546-558.
49. Zhang, Q.; Wilson, P.; Li, Z.; McHale, R.; Godfrey, J.; Anastasaki, A.; Waldron, C.; Haddleton, D. M. Aqueous Copper-Mediated Living Polymerization: Exploiting Rapid Disproportionation of CuBr with Me6TREN. *J. Am. Chem. Soc.* **2013,** 135 (19), 7355-7363.

50. Rademacher, J. T.; Baum, M.; Pallack, M. E.; Brittain, W. J.; Simonsick, W. J. Atom Transfer Radical Polymerization of N,N-Dimethylacrylamide. *Macromolecules* **2000,** 33 (2), 284-288.
51. Figg, C. A.; Simula, A.; Gebre, K. A.; Tucker, B. S.; Haddleton, D. M.; Sumerlin, B. S. Polymerization-induced thermal self-assembly (PITSA). *Chem. Sci.* **2015,** 6 (2), 1230-1236.
52. Whittaker, V. P. An experimental investigation of the "ring hypothesis" of arsenical toxicity. *Biochem. J.* **1947,** 41 (1), 56-62.
53. Friedheim, E. A. H. Substituted 1,3,5-triazinyl-(6)-aminophenyl-arsenic compounds. United States Patent, US2422724 A, 1947.
54. Tande, B. M.; Wagner, N. J.; Mackay, M. E.; Hawker, C. J.; Jeong, M. Viscosimetric, Hydrodynamic, and Conformational Properties of Dendrimers and Dendrons. *Macromolecules* **2001,** 34 (24), 8580-8585.
55. Brewer, A. K.; Striegel, A. M. Characterizing the size, shape, and compactness of a polydisperse prolate ellipsoidal particle via quadruple-detector hydrodynamic chromatography. *Analyst* **2011,** 136 (3), 515-519.
56. Adams, E.; Jeter, D.; Cordes, A. W.; Kolis, J. W. Chemistry of organometalloid complexes with potential antidotes: structure of an organoarsenic(III) dithiolate ring. *Inorg. Chem.* **1990,** 29 (8), 1500-1503.
57. Rheingold, A. L.; Sullivan, P. J. Crystal and molecular structure of hexaphenylcyclohexaarsine, c-(AsPh)6. *Organometallics* **1983,** 2 (2), 327-331.
58. Aposhian, H. V.; Zakharyan, R. A.; Avram, M. D.; Kopplin, M. J.; Wollenberg, M. L. Oxidation and detoxification of trivalent arsenic species. *Toxicol. Appl. Pharmacol.* **2003,** 193 (1), 1-8.
59. Naranmandura, H.; Suzuki, N.; Iwata, K.; Hirano, S.; Suzuki, T. Arsenic Metabolism and Thioarsenicals in Hamsters and Rats. *Chem. Res. Toxicol.* **2007,** 20 (4), 616-624.
60. Zamora, P. L.; Rockenbauer, A.; Villamena, F. A. Radical Model of Arsenic(III) Toxicity: Theoretical and EPR Spin Trapping Studies. *Chem. Res. Toxicol.* **2014,** 27 (5), 765-774.
61. Di Cara, F.; Sheshachalam, A.; Braverman, N. E.; Rachubinski, R. A.; Simmonds, A. J. Peroxisome-Mediated Metabolism Is Required for Immune Response to Microbial Infection. *Immunity* **2017,** 47 (1), 93-106.
62. Lennicke, C.; Rahn, J.; Lichtenfels, R.; Wessjohann, L. A.; Seliger, B. Hydrogen peroxide – production, fate and role in redox signaling of tumor cells. *Cell Commun. Signaling* **2015,** 13, 39.